De Gruyter Brill
Paradigm
ISSN 1335-8871

MEASUREMENT SCIENCE REVIEW

Journal homepage: https://reference-global.com/journal/MSR

A New Low-Noise X-Ray Imaging Detector

Liping Tian[2], Yang Yang[1], Lingbin Shen[2], Penghui Feng[1], Bo Wang[1], Yan Xu[1], Jinshou Tian[1], Yongsheng Gou[1*]

[1]*State Key Laboratory of Ultrafast Optical Science and Technology, Key Laboratory of Ultra-fast Photoelectric Diagnostics Technology, Xi'an Institute of Optics and Precision Mechanics, Chinese Academy of Sciences, Xi'an, 710119, China, yshgou@163.com*
[2]*School of Network and Communication Engineering, Jinling Institute of Technology, Hongjing Road, No. 99, Nanjing, 211169, China, tianliping@jit.edu.cn*

Abstract: A newly proposed low-noise and high temporal resolution X-ray imaging detector based on the curved solenoid design is described in this paper. Three-dimensional models are developed in CST Particle Studio (CST-PS) to systematically investigate the temporal and spatial magnifications. The effects of the ramp rate of the modulation signal between the photocathode and the acceleration mesh, the different electron emission positions of the photocathode, the magnetic field strength, and the distance between the microchannel plate (MCP) and the curved solenoid outlet on the overall performance of the whole structure are studied, which shows that the electron emission position has a dominant effect over the temporal transit and temporal dispersion. Additionally, the temporal magnification factor increases with the ramp rate of the modulated signal. Within the effective photocathode of Φ16 mm, the temporal magnification factor exceeds 13. Furthermore, the spatial magnification is linearly proportional to the distance between the MCP and the solenoid outlet, suggesting that MCPs of varying sizes can be effectively coupled.

Keywords: curved solenoid, temporal magnification, X-ray detector

1. INTRODUCTION

X-ray detectors are a well-established instrument used in large scientific devices, including large-scale laser systems and high-energy ion beam facilities [1]-[3]. Microchannel plate (MCP) providing both high gain, high sensitivity, and small size is a promising electron multiplier device, especially in night vision and single particle aerosol mass spectrometry [4]-[6]. The x-ray detector based on MCP offers advantages such as a rapid response time and direct detection capabilities [7]-[9]. This technology can effectively detect the instantaneous emission of X-ray signals generated by high-energy-density materials, facilitating the diagnosis of their parameters [10]. However, the neutron signal accompanying the X-ray signal is both time-synchronized and spatially aligned. Components of an X-ray detector, including the cathode and MCP, are capable of responding to neutrons. At the same time, the interaction of high-energy neutrons with the materials comprising the X-ray detector generates secondary radiation and associated effects. The resultant high background and elevated noise levels produced by these neutrons adversely affect the signal-to-noise ratio (SNR) of the X-ray detector and may also inflict permanent damage to the detector itself. Although shielding technology for harmful neutron radiation has advanced significantly, the extraction of optoelectronic signals generated by X-ray signals concurrently and spatially amid a strong neutron radiation background remains underexplored and unreported in the literature.

In this paper, we present the design of a compact, low-noise X-ray detector with high temporal resolution, specifically designed to extract X-rays from a strong radiation background. This objective is accomplished by substituting conventional solenoids with 90-degree bent solenoids. This innovation of different coaxial designs of the cathode and MCP also results in a lower noise floor, which is essential for the detection of X-ray photons.

2. CONCEPT DESIGN AND SIMULATION DETAILS

To obtain optoelectronic information against a backdrop of intense radiation, a novel X-ray detector with a curved solenoid is proposed in this paper. The schematic diagram is presented in Fig. 1 (lower section). Compared to the existing X-ray detector (upper section) [11]-[14], the structure of the new design has undergone significant changes. The new detector comprises a photocathode, an acceleration mesh, a curved solenoid, and an MCP detection screen. All

DOI: 10.2478/msr-2026-0006

*Corresponding author: yshgou@163.com (Yongsheng Gou)

components are situated within a high-vacuum chamber, and the dimensions of this compact structure are just 110 mm × 110 mm. A 1 mm accelerating gap is established between the photocathode and the mesh to create a high acceleration field, with the ultra-fine mesh exhibiting a transmittance of approximately 60 %. The drift solenoid is designed in a quarter-spherical form, mainly to isolate high-energy neutron signals. The X-ray activates the photocathode, resulting in the emission of electrons that are proportional to the light intensity. Subsequently, these electrons are accelerated into an angle-sensitive detector or through a 90-degree bent solenoid, facilitated by accelerating and electronic drift electrodes. Ultimately, the photoelectrons enter the MCP for multiplication. Notably, the directions of electron emission and light incidence are perpendicular, which helps prevent direct penetration of light and stray particles, thereby reducing noise. This paper focuses exclusively on the electron transport from the photocathode to the input surface of the MCP and does not address the electron multiplication within the MCP, as this topic has been extensively studied. It is important to note that in the CST modeling, ten hollow cylindrical solenoids are bent at an angle of 10 degrees to create the electronically drifted section of the 90-degree bent solenoid, as shown in Fig. 1 (lower section). The applied voltage distribution is presented in Table 1.

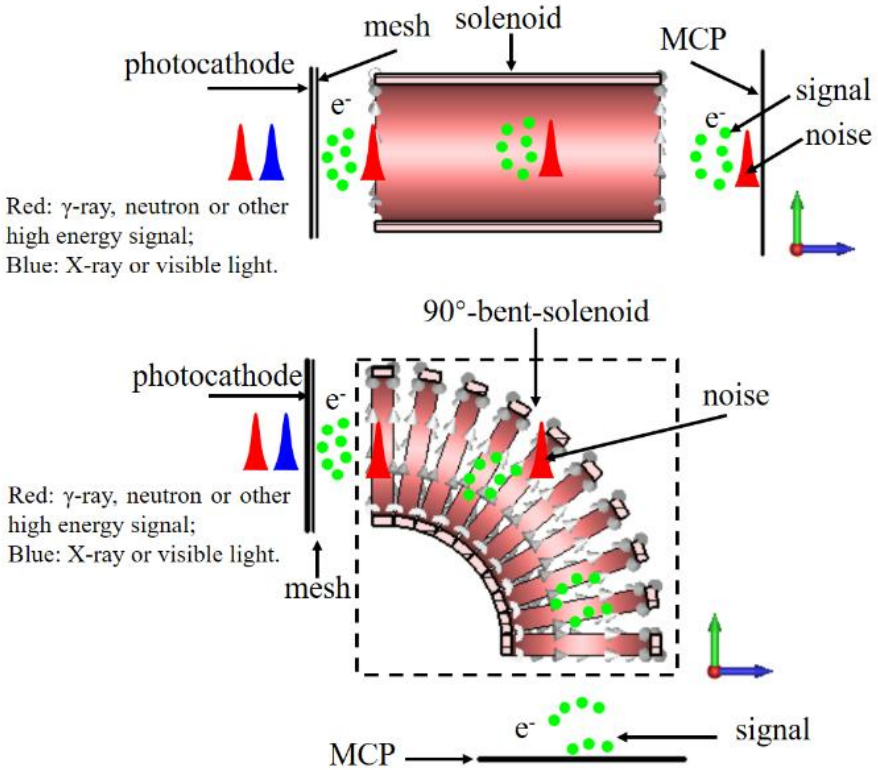

Fig. 1. Schematic diagram of the traditional (upper) and novel (lower) X-ray detector.

Table 1. Voltage and current parameter distribution.

Components	Voltage [V]			Number of single turns	Current of turns [A]
	Photocathode	Mesh	MCP		
Parameters	–1200	–300	0	40	200

3. Simulation Results and Discussions

A. Electromagnetic field distribution

The electric and magnetic field distributions at various off-axis distances in this novel low-noise X-ray detector were calculated using the finite integral method, as illustrated in Fig. 2. The strong electric field between the cathode and acceleration mesh imparts energy to the photoelectrons, while the curved solenoid magnetic field alters the trajectories of the photoelectrons. However, for high-energy neutrons, the strong electric and magnetic fields have no significant effect. Nonetheless, this bent solenoid structure can effectively reduce background noise generated by high-energy neutrons.

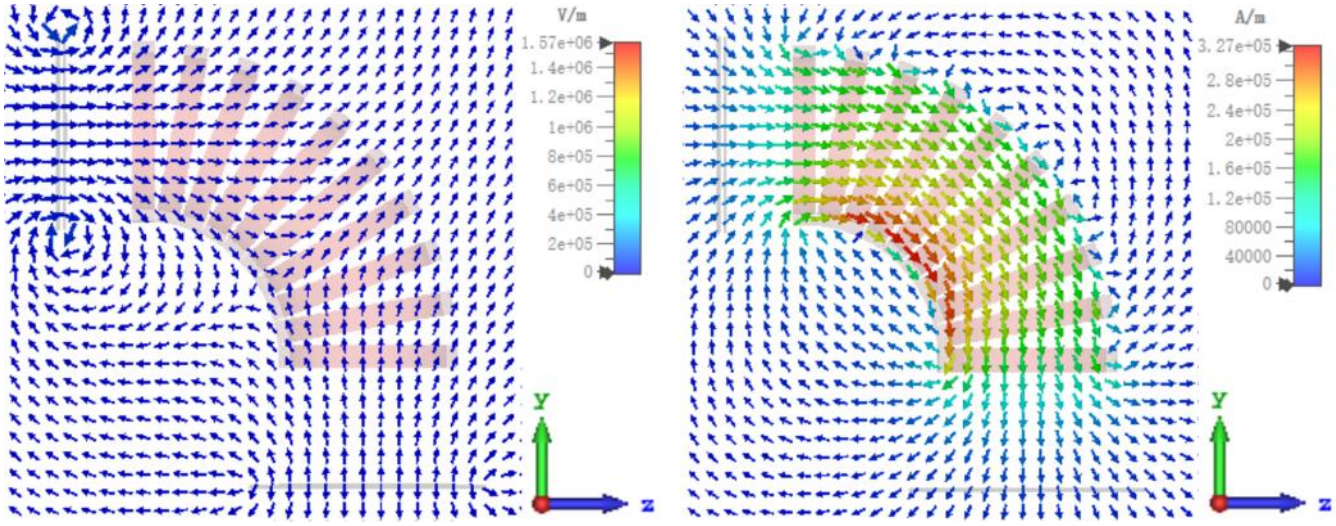

(a) (b)

Fig. 2. Electromagnetic field distribution. (a) Electric field distribution; (b) Magnetic field distribution.

B. Transit time distribution

Due to the variations in axial electric and magnetic fields as well as the operating paths, the transition time of photoelectrons emitted from the photocathode is approximately several hundred ps. Fig. 3 shows the trajectories of the photoelectrons across the entire photocathode. Fig. 4 presents the transit time distribution of the photoelectrons at various off-axis distances, ranging from –10 mm to 10 mm (corresponding to a photocathode diameter of 20 mm). The simulation results indicate that the overall transit time of the tube is about 10 ns, with a transit time spread of approximately 1 ns. The optimal value occurs at $x = -2$ mm, where the transit time and transit time spread of the detector are 8.77 ns and 29 ps, respectively.

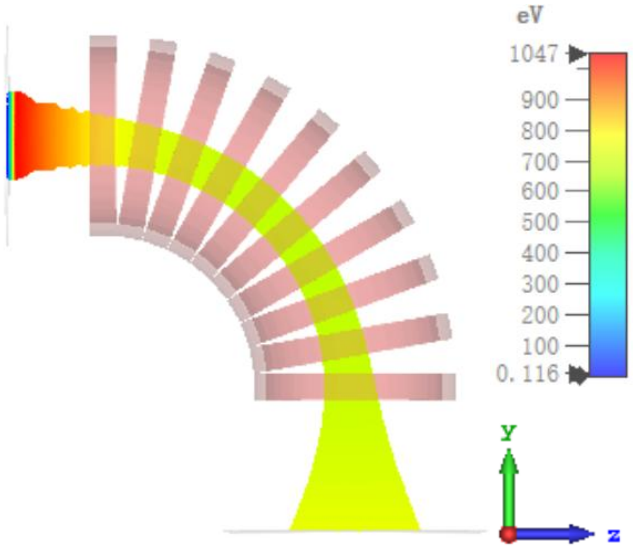

Fig. 3. Photoelectron trajectories from the whole photocathode.

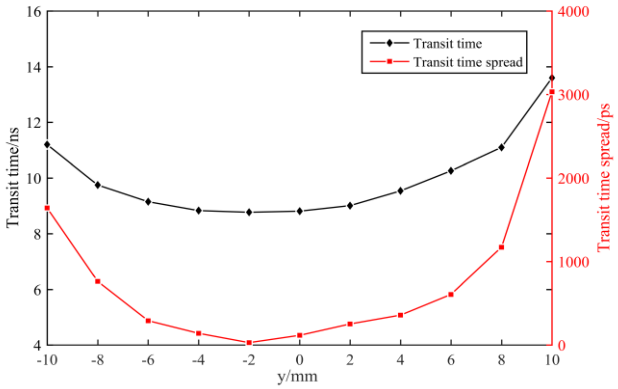

Fig. 4. Transit time and transit time spread versus the photocathode positions (slit direction).

C. Temporal resolution modulation factor

The electron-pulse dilation is the result of the driven pulse applied to the photocathode and the accelerating mesh. The temporal magnification M from the cathode to the input surface of the MCP can be estimated by

$$M = 1 + \frac{L}{t_2 - t_1}\left\{\frac{L}{\sqrt{2e/m}}\left(\frac{1}{\sqrt{u_2}} - \frac{1}{\sqrt{u_1}}\right)\right\} \quad (1)$$

$$u_2 = u_1 - k(t_2 - t_1) \quad (2)$$

where L is the length of the electron drift region, t_2 and t_1 are the times at which the electron beam front and end enter the solenoid, respectively. e is the electron charge and m is the electron mass. k is the gradient of the ramp pulse unit in V/ps.

3D particle-in-cell (PIC) simulations were conducted to assess the temporal magnification of the X-ray detector. The X-ray detector, which features a negative time-varying potential applied to the photocathode-accelerating mesh gap, has a ramp rate of 5, 10, 15, 20, and 25 V/ps. This configuration was chosen to emit photoelectrons with both initial

energy dispersion and directional dispersion from the center of the photocathode. This setup was used to observe the influence of the modulation ramp rate on the time magnification of the X-ray detector. Fig. 6 illustrates the time magnification at the object point located at the center of the photocathode under various modulation pulsed ramp rates. From Fig. 5, it can be concluded that, due to the electromagnetic field of the bending structure drift systems, the time magnification is smallest at $x = -2$ mm, rather than at the center of the photocathode.

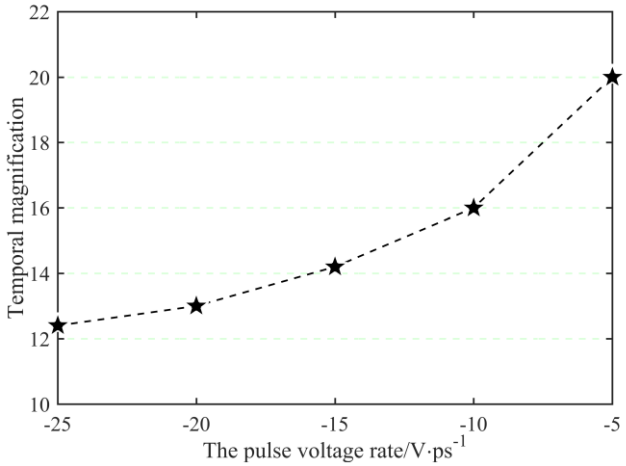

Fig. 5. Temporal magnification versus the ramped pulsed ramp rate.

Temporal magnification versus the distance from the photocathode center is shown in Fig. 6. It is obvious that the temporal magnification increases with the increasing distance. Temporal magnifications of the X-ray detector at different photocathode distances are all higher than 13. With the enlargement of the photoelectron emission region, the uniformity of the electromagnetic field intensity becomes worse, thereby affecting the trajectory of the electrons, which in turn affects the temporal magnification. The lowest temporal magnification is 13.8 at an off-axis distance of –2 mm. The temporal magnification difference of all the calculated photocathode distances is no more than 0.95, which implies good uniformity. Combining Fig. 4 and Fig. 6, the effective photocathode area of the X-ray detector is of Φ16 mm.

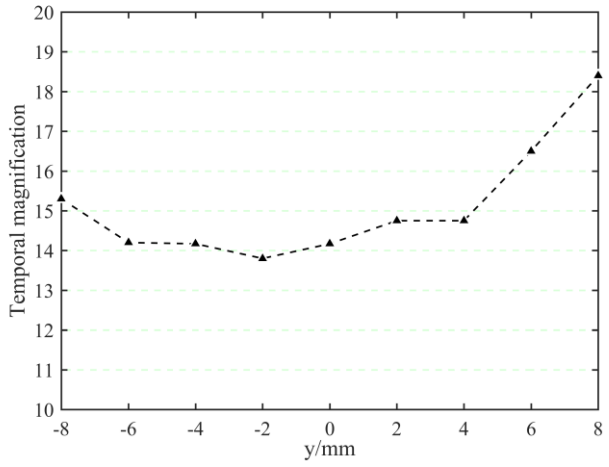

Fig. 6. Temporal magnification versus the photocathode illuminated position.

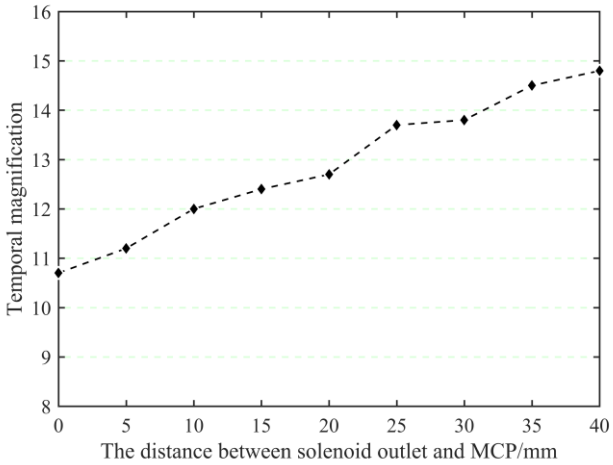

Fig. 7. Temporal magnification versus the distance between the solenoid outlet and the MCP.

Fig. 7 displays the temporal magnification variation with the distance d, which is defined as the distance between the solenoid outlet and the input surface of the MCP. It can be seen that the temporal magnification increases with the d and the simulating curve follows (1). When the distance d is increased from 0 mm to 40 mm by step of 5 mm, the temporal magnification increases from 10.7 to 14.8. This increase can be attributed primarily to the extended travel distance of the photoelectrons in the drift region.

In the 3D model, a ramp rate of the modulation pulse voltage of 15 V/ps was applied between the photocathode and the accelerating mesh. Two electron pulses with a size of Φ2 mm are emitted at a distance of 2 mm from the center of the photocathode (specifically at $x = -2$ mm). The interval between pulses is 60 ps, with a half-height and full width of 1 ps. The study investigates the time amplification of electrons at the MCP detection screen located 2 mm from the center of the photocathode ($x = -2$ mm), comparing scenarios with and without modulation pulses. Fig. 8 presents the simulation results, which indicate that in the absence of modulation pulses, the cathodic electrons accumulate due to time dispersion. Conversely, when modulation pulses are applied, the two electron pulses broaden from 60 ps to 830.4 ps, resulting in a time amplification factor of 13.8.

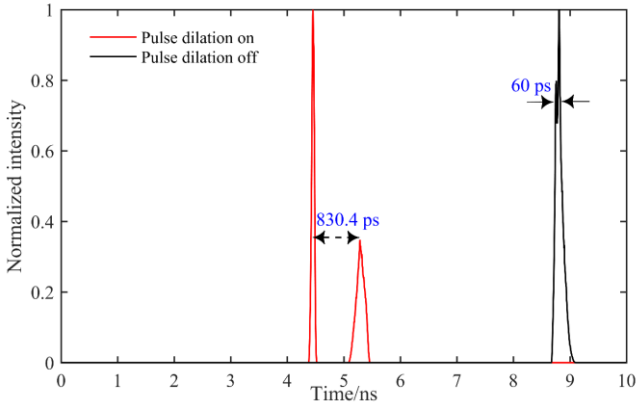

Fig. 8. Comparison of dilated vs non-dilated signal for input double peaks separated by 60 ps.

Fig. 9 shows the corresponding temporal magnification factor when the photoelectrons emitted from the center of the cathode are subjected to various magnetic fields under the condition of a modulation signal ramp rate of 15 V/ps. As the magnetic field strength increases, the time amplification factor remains almost unchanged.

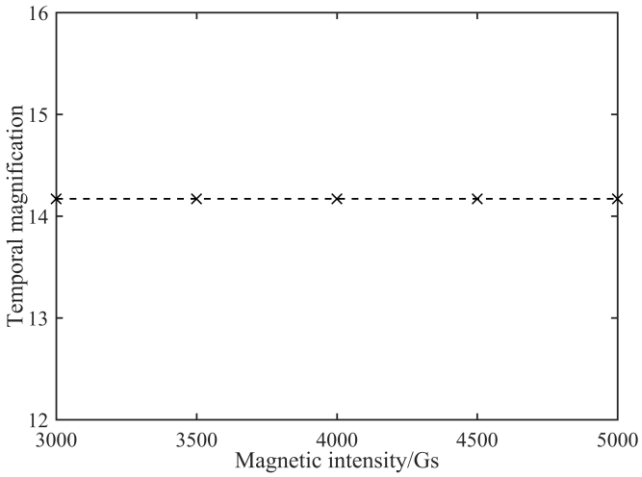

Fig. 9. Magnification versus the magnetic intensity.

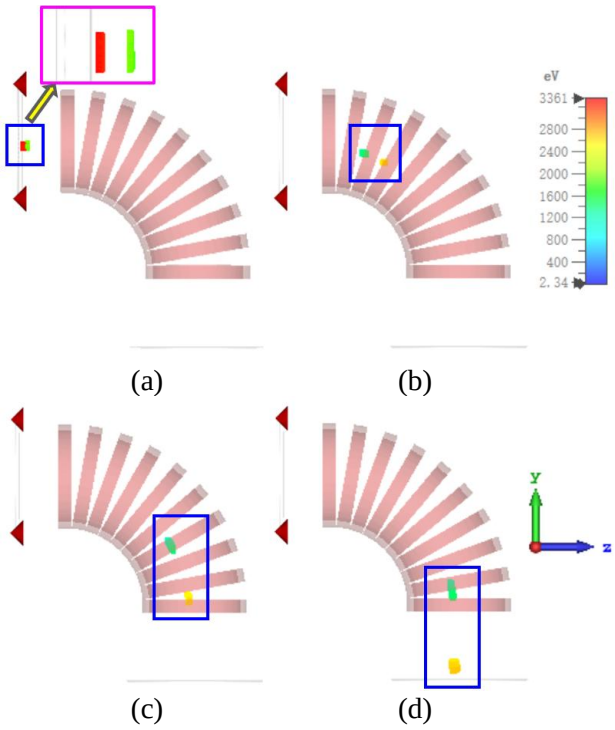

Fig. 10. Demonstration of electric trajectory: (a) $t = 230\ ps$; (b) $t = 1640\ ps$; (c) $t = 3740\ ps$; (d) $t = 4520\ ps$.

Fig. 10 shows the trajectories of photoelectron pulses at four distinct time intervals. Fig. 10(a) displays the electron trajectories at $t_1 = 230$ ps, during which the two photoelectron pulses orbit near the photocathode with a time interval of 60 ps. Fig. 10(b) shows the moment when the photoelectrons enter the inlet of the drift solenoid, occurring at $t_2 = 1640$ ps, where the effect of photoelectron time dilation is minimal. Fig. 10(c) presents the trajectory of the photoelectrons at the outlet of the drift solenoid, at $t_3 = 3740$ ps, where the photoelectron dilation effect becomes pronounced. Finally, Fig. 10(d) presents the photoelectron trajectory at $t_4 = 4520$ ps, at which point the time dilation effect is most significant as the photoelectrons approach the MCP detection screen.

D. The spatial magnification

To couple MCPs of varying sizes, we investigated the spatial magnification between the solenoid outlet and the MCPs as a function of different distances. In our simulation, the electron source is emitted from the Φ16 mm photocathode. The relationship between spatial magnification and d is illustrated in Fig. 11. The results indicate that spatial magnification increases almost linearly with spacing, reaching a value of 1 when the spacing is 15 mm.

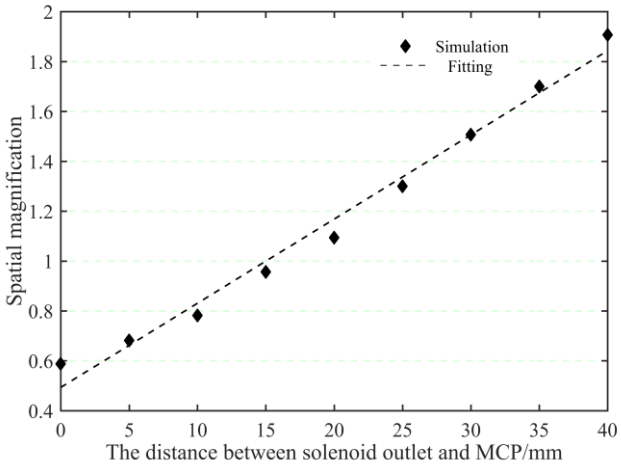

Fig. 11. Spatial magnification versus the distance between the solenoid outlet and the MCP.

4. CONCLUSION

In this work, a novel X-ray detector based on a curved solenoid is designed using three-dimensional electromagnetic simulation software, CST Particle Studio (CST-PS). The X-ray detector consists of a photocathode, an accelerating mesh, a curved solenoid, and the MCP multiplication system. As an electronic guidance device, the curved solenoid can pass the background noise of high-energy neutrons, enabling X-ray detection with high signal-to-noise ratios in high-energy particle detection environments. The effective working area of the X-ray detector is greater than Φ16 mm. The temporal magnification is related to the position of the electrons emitted from the photocathode. The temporal magnification in the entire working area exceeds 13, and the magnetic field strength has almost no effect on the temporal amplification. Furthermore, as the ramp rate of the modulated signal between the photocathode and accelerating mesh increases, the temporal magnification rises correspondingly, indicating that the ramp rate of the modulated signal has a pronounced effect on this factor. The spatial magnification of this X-ray detector is linearly positively correlated with the distance between the MCP and the outlet of the magnetic lens,

allowing for easy matching of MCPs of different sizes. This study offers valuable guidance for detecting ultrafast X-ray signals in high-energy background environments.

ACKNOWLEDGMENT

This study is supported by the National Natural Science Foundation of China (Grant No. 12405246).

REFERENCES

[1] Wang, Q., Cao, Z., Chen, T., Deng, B., Deng, K., Tian, J. (2021). Numerical study and improvement of the dynamic performance of dilation x-ray imager. *Review of Scientific Instruments*, 92 (12), 123305. https://doi.org/10.1063/5.0061685

[2] Cai, H., Luo, Q., Lin, K., Deng, X., Liu, J., Yang, K., Wang, D., Chen, J., Wang, J., Long, J., Niu, L., Lei, Y., Liu, J. (2024). Ultrafast pulse-dilation framing camera and its application for time-resolved X-ray diagnostic. *Nuclear Science and Techniques*, 35, 126. https://doi.org/10.1007/s41365-024-01408-2

[3] Fu, W., Hu, C., Chen, P., Zhou, R., Li, L. (2024). The development of an electron pulse dilation photomultiplier tube diagnostic instrument. *Sensors*, 24 (23), 7497. https://doi.org/10.3390/s24237497

[4] Han, B., Gao, W., Feng, J., Iroshan, A., Yang, J., Chen, G., Zhang, Y., Aizezi, N., Liu, Y. (2025). Laser-induced breakdown spectroscopy for imaging and distribution analysis of heavy metal elements in soil. *Journal of Hazardous Materials*, 496, 139284 https://doi.org/10.1016/j.jhazmat.2025.139284

[5] Chen, L., Zhang, B., Liu, S., Yan, B., Peng, H., Zhang, Y., Luo, T. (2025). Optimization study on the collection efficiency of the channel electron multiplier in a UV photoelectron spectroscopy analyzer. *Optics Continuum*, 4 (5), 1030-1039. https://doi.org/10.1364/OPTCON.550311

[6] Ye, Y., Aizezi, N., Feng, J., Han, B., Li, X., Su, Z., Liu, Y. (2025). Advanced characterization of industrial smoke: Particle composition and size analysis with single particle aerosol mass spectrometry and optimized machine learning. *Analytical Chemistry*, 97 (10) 5554-5562. https://doi.org/10.1021/acs.analchem.4c05988

[7] Gales, S. G., Horsfield, C. J., Meadowcroft, A. L., Leatherland, A. E., Herrmann, H. W., Hares, J. D., Dymoke-Bradshaw, A. K. L., Milnes, J. S., Kim, Y. H., Kleinrath, H. G., Meaney, K., Zylstra, A. B., Parke, S., Hussey, D., Wilson, L., James, S. F., Kilkenny, J. D., Hilsabeck T. J. (2018). Characterisation of a sub-20 ps temporal resolution pulse dilation photomultiplier tube. *Review of Scientific Instruments*, 89 (6), 063506. https://doi.org/10.1063/1.5031110

[8] Fu, W., Huang, J., Wang, D., Lei, Y., Wang, Y., Deng, P., Long, J., Cai, H., Liu, J. (2020). Development of an ultra-fast photomultiplier tube with pulse-dilation technology. *IEEE Access*, 8, 47533-47537. https://ieeexplore.ieee.org/document/9031430

[9] Dymoke-Bradshaw, A. K. L., Hares, J. D., Milnes, J., Herrmann, H. W., Horsfield, C. J., Gales, S. G., Leatherland, A., Hilsabeck, T., Kilkenny, J. D. (2018). Development of an ultra-fast photomultiplier tube for gamma-ray Cherenkov detectors at the National Ignition Facility (PD-PMT). *Review of Scientific Instruments*, 89 (10), 10I137. https://doi.org/10.1063/1.5039327

[10] Herrmann, H. W., Kim, Y. H., McEvoy, A. M., Zylstra, A. B., Young, C. S., Lopez, F. E., Griego, J. R., Fatherley, V. E., Oertel, J. A., Stoeffl, W., Khater, H., Hernandez, J. E., Carpenter, A., Rubery, M. S., Horsfield, C. J., Gales, S., Leatherland, A., Hilsabeck, T., Kilkenny, J. D., Malone, R. M., Hares, J. D., Milnes, J., Shmayda, W. T., Stoeckl, C., Batha, S. H. (2016). Next generation gamma-ray Cherenkov detectors for the National Ignition Facility. *Review of Scientific Instruments*, 87 (11), 11E732. https://doi.org/10.1063/1.4962059

[11] Bai, Y., Yao, R., Gao, H., Wang, X., Liu, D. (2020). Measurement of dilation pulses using a pulse-dilation framing camera. *Optics Express*, 28 (10), 15407-15415. https://doi.org/10.1364/OE.391779

[12] Fu, W., Luo, Q., Huang, J., Huang, J., Duan, X., Liao, Y., Liu, J., Xiang, L., Cai, H. (2024). An ultrafast x-ray diode with electronic pulse-dilation technique. *IEEE Sensors Journal*, 24 (4), 4442-4448. https://ieeexplore.ieee.org/document/10382430

[13] Trosseille, C., Nagel, S. R., Hilsabeck, T. J. (2023). Electron pulse-dilation diagnostic instruments. *Review of Scientific Instruments*, 94 (2), 021102. https://doi.org/10.1063/5.0128802

[14] Nagel, S. R., Hilsabeck, T. J., Bell, P. M., Bradley, D. K., Ayers, M. J., Piston, K., Felker, B., Kilkenny, J. D., Chung, T., Sammuli, B., Hares, J. D., Dymoke-Bradshaw, A. K. L. (2014). Investigating high speed phenomena in laser plasma interactions using dilation x-ray imager (invited). *Review of Scientific Instruments*, 85 (11), 11E504. http://dx.doi.org/10.1063/1.4890396

Received May 2, 2025
Accepted November 21, 2025